Title: Motor Protein MYO1C is Critical for Photoreceptor Opsin Trafficking and Vision

Authors: Ashish K. Solanki[1], Elisabeth Obert[2], Stephen Walterhouse[1], Ehtesham Arif[1], Bushra Rahman[1], Joshua H. Lipschutz[1,3], Jeffery Sundstrom[4], Barbel Rohrer[2,3], Shahid Husain[2], Glenn P. Lobo[1,2]* and Deepak Nihalani[1]*

Affiliations: [1]Department of Medicine, Medical University of South Carolina, Charleston, SC, 29425, USA. [2]Department of Ophthalmology, Medical University of South Carolina, Charleston, SC, 29425, USA. [3]Ralph H. Johnson VA Medical Center, Division of Research, Charleston, SC 29420, USA. [4]Penn State Eye Center, 200 Campus Dr., Suite 800, Hershey, PA 17033. USA.

***Corresponding Authors**
***Glenn P. Lobo, Ph.D.**
Assistant Professor of Medicine
Department of Medicine
70 President Road
Drug Discovery Building DDB513
Charleston, SC 29425
Office: 843-876-2371
Fax: 843-792-8399
Email: lobo@musc.edu

***Deepak Nihalani, Ph.D.**
Associate Professor of Medicine
Department of Medicine
70 President Road
Drug Discovery Building DDB514
Charleston, SC 29425
Office: 843-792-7659
Fax: 843-792-8399
Email: nihalani@musc.edu

Keywords: Motor protein, Myosin, MYO1C, Opsins, Photoreceptor, Outer Segments, Photoreceptor Cell Degeneration, Trafficking, Vision.

Abstract

Unconventional myosins linked to deafness are also proposed to play a role in retinal physiology. However, their direct role in photoreceptor structure and function remains unclear. Herein, we demonstrate that systemic loss of the unconventional myosin MYO1C in mice affected opsin trafficking and photoreceptor survival, leading to vision loss. Electroretinogram analysis of *Myo1c* knockout (*Myo1c*-KO) mice showed a progressive loss of rod and cone function. Immunohistochemistry and binding assays demonstrated MYO1C localization to photoreceptor inner and outer segments (OS) and identified a direct interaction of rhodopsin with the MYO1C cargo domain. In *Myo1c*-KO retinas, rhodopsin mislocalized to rod inner segments and the cell bodies, while cone opsins in OS showed punctate staining. In aged mice, the histological and ultrastructural examination of *Myo1c*-KO retinas showed a progressively degenerating photoreceptor OS phenotype. These results demonstrate that MYO1C is critical for opsin trafficking to the photoreceptor OS and normal visual function.

Introduction

Protein trafficking within the photoreceptors must occur efficiently and at high fidelity for photoreception, structural maintenance and overall retinal cell homeostasis. Additionally, it is well known that proper opsin trafficking is tightly coupled to photoreceptor cell survival and function [1-9]. However, the cellular events, including signaling pathways and trafficking events that participate in retinal injuries due to improper protein trafficking to the photoreceptor outer segments (OS), are not yet fully understood. While many proteins are known to play an essential role in retinal cell development and function, the involvement of motor proteins in eye biology is less understood. Identification of genetic mutations in the *Myo7a* gene associated with retinal degeneration in Usher syndrome suggests that unconventional myosins play a critical role in retinal pigmented epithelium (RPE) and photoreceptor cell function [10, 11]. Unconventional myosins are motor proteins that are proposed to transport membranous organelles along the actin filaments in an ATP-dependent manner, and additional roles are currently being uncovered [12-14]. The loss of *Myo7a* primarily affects RPE and OS phagocytosis leading to retinal cell degeneration. It is, however, believed that other, yet unidentified class I myosins, may participate more directly in photoreceptor function. Here we present compelling evidence for another unconventional actin-based motor protein, MYO1C, with its primary localization to photoreceptors, that plays a role in retinal cell structure and function via opsins trafficking to the photoreceptor OS.

Rhodopsin and cone pigments in photoreceptor OS mediate scotopic and photopic vision, respectively. They consist of opsin, the apo-protein, and 11-*cis* retinal, a

vitamin A-based chromophore. Light absorption by 11-*cis* retinal triggers a conformational change in opsin [8]. This, in turn, initiates a G protein-coupled receptor (GPCR) signaling pathway/phototransduction cascade, signaling the presence of light. Thus, the presence of opsins in the photoreceptor OS is critical for vision [1-9]. Each photoreceptor cell contains an OS housing the phototransduction machinery, an inner segment (IS) where proteins are biosynthesized and energy is being produced, and a synaptic terminal for signal transmission. One of the most fundamental steps in vision is the proper assembly of signal-transducing membranes, including the transport and sorting of protein components. A major cause of neurodegenerative and other inherited retinal disorders is the improper localization of proteins. Mislocalization of the dim-light photoreceptor protein rhodopsin is a phenotype observed in many forms of the blinding disease, including retinitis pigmentosa. The proteins that participate in phototransduction (including rhodopsin, transducin, phosphodiesterase [PDE6], or the cyclic nucleotide gated channels [CNG], are synthesized in the IS and must be transported through the connecting cilium (CC) to the OS. These proteins are either transmembrane (TM) proteins or peripherally associated membrane proteins that are attached to the membrane surface [1-9]. How the TM proteins (e.g., rhodopsin and CNG) and peripherally associated proteins (e.g., transducin and PDE6) traffic through the IS to incorporate eventually in the nascent disc membrane or the photoreceptor outer membrane is not fully understood and constitutes an area of intense research, as improper trafficking of these protein causes retinal cell degeneration and can lead to blindness [1-9].

Genetic mutations in myosins that lead to hearing loss have also been associated with retinal degeneration. Some of the essential genes known to be involved in either or both of these functions belong to a family of unconventional motor proteins and include MYO3A [15], MYO7A , MYO6 , MYO15 [16], and MYO5. A recent report identified another unconventional myosin associated with deafness, MYO1C, where mutations which affects its nucleotide-binding pocket and calcium binding ability [17]. Importantly, MYO1C was identified in the proteomic analysis of the retina and vitreous fluid as part of a protein hub involved in oxidative stress [18-20]. MYO1C is an actin-binding motor protein that is widely expressed in multiple cell types. It has been shown to participate in a variety of cellular functions including protein trafficking and translocation [12, 21-23]. As MYO1C has low tissue specificity based on mRNA and protein expression, it remains unclear which cell type is most dependent on MYO1C trafficking function and is affected by the loss of MYO1C.

In this study, we aimed to systematically analyze the function of the motor protein MYO1C in protein trafficking in photoreceptors. Here, we find that a global genetic deletion of *Myo1c* results in progressive mistrafficking of opsins to the OS. Using retinal lysate from wild-type (WT) mice in co-immunoprecipitation assays, we show that MYO1C and rhodopsin directly interact, indicating that opsin is a cargo for MYO1C. Loss of MYO1C promoted a progressive OS degeneration concomitant with a reduction in rod and cone photoreceptor cell function, suggesting that MYO1C is critical for retinal structure and function. Our findings have significant clinical implications for degenerative rod and cone diseases, as mutations in MYO1C or its interacting partners

could exert its effects on retinal health and vision by altering opsin trafficking to the photoreceptor OS, a fundamental step for maintaining vision in humans.

Results

Construction and Validation of *Myo1c* null Mice*:* We have previously generated *Myo1c* floxed mice using the standard knockout strategy [24]. Systemic deletion of *Myo1c* was achieved by crossing *Myo1c* floxed (*Myo1cfl/fl*) mice with Actin Cre+ (ActCre+) mice to generate *Myo1cfl/fl ActCre+/-* knockout mice (referred to as *Myo1c*-KO mice in this manuscript). Western blotting of protein lysates from various tissues including kidney, heart, and liver of *Myo1c*-KO mice showed complete loss of MYO1C, thus confirming the systemic deletion of *Myo1c* (**Fig. S1a**). Additionally, immunostaining analysis of these tissues further confirmed loss of MYO1C protein in *Myo1c*-KO mice (**Figs. S2a-d**).

Genetic Deletion of *Myo1c* induces Visual Impairment in Mice: Immunofluorescence analysis showed that MYO1C was enriched in the OS and IS of WT mice and absent in *Myo1c*-KO retinas (**Fig. 1a**). Since mutations or deletion of the motor protein MYO7A has been associated with retinal degeneration in Usher syndrome or its animal model respectively, it prompted us to investigate whether *Myo1c* deletion affects retinal function. Using electroretinograms (ERGs) [25, 26], we tested photoreceptor cell function of *Myo1c*-KO and WT mice (*n*=8, per genotype and age-group) under dark-adapted, scotopic and light-adapted, photopic conditions to

determine rod and cone function, respectively. In contrast to WT animals, we observed reduced ERGs for *Myo1c*-KO mice at different ages. Two months old *Myo1c*-KO mice showed significant reduction in the ***a***-wave but not ***b***-wave amplitudes ($P<0.0068$ and $P<0.098$, respectively) (**Figs. 1b-c**). Strikingly, ERG analysis of adult six months old *Myo1c*-KO mice showed severe loss of retinal function, where a significant reduction in both ***a***- and ***b***-waves was observed (38-45% of WT animals ($P<0.005$)) (**Figs. 1d-e**). These analyses suggest the absence of key phototransduction components in the photoreceptor OS of *Myo1c*-KO mice and/or photoreceptor OS degeneration, as contributing factors.

Rod and Cone Visual Pigments in *Myo1c*-KO Mice: Since, the phototransduction protein, rhodopsin, constitutes 85-90% of photoreceptor OS protein content [27], and as the ERG responses were impaired in *Myo1c*-KO mice, we hypothesized that the loss of MYO1C may affect opsin trafficking to the photoreceptor OS. To test this hypothesis, we analyzed retinal sections from WT and *Myo1c*-KO mice (at 2 and 6 months of age; $n=8$ per genotype), probing for rhodopsin, two types of cone opsins (red/green (medium wavelength, M-opsin and S-opsin (short wavelength)), rod-specific phosphodiesterase 6b (Pde6b) and a general cone marker, PNA lectin. In WT mice, rhodopsin localized exclusively to the rod outer segments at 2 and 6 months of age. In contrast, in two months old *Myo1c*-KO mouse retinas, while most rhodopsin trafficked to the OS, some also mislocalized to the base of the rod IS and the cell bodies in the outer nuclear layer (ONL), suggesting incomplete target transport/trafficking to photoreceptor OS in the absence of MYO1C (**Fig. 2a;** white arrows; rhodopsin levels within individual retinal

layers are quantified and shown in **Fig. S3**). An even more severe mislocalization of rhodopsin to the rod IS, and within the ONL was observed in the 6 months old *Myo1c*-KO mice, suggesting a progressive retinal phenotype in the absence of MYO1C (**Fig. 2a;** rhodopsin expression within individual retinal layers are quantified and shown in **Fig. S4**). In contrast, staining for Pde6b, a lipidated rod specific protein that does traffic to OS independently of rhodopsin [28], showed normal trafficking to the rod OS in both WT and *Myo1c*-KO retinas (**Fig. 2d**). Staining for the two cone opsins suggests that the cone outer segments are shorter and swollen by 2 and increasingly so by 6 months of age (**Figs. 2b-c**). This observation is supported by staining for PNA lectin, documenting progressively shorter and fatter cone OS, indicative that cone OS degenerate as these mice age in the absence of MYO1C (**Fig. 2e**). Cone visual arrestin in WT mice typically outlines the entire cell, OS, IS, cell body, axon and cone pedicle. Staining for cone arrestin in *Myo1c*-KO animals confirmed the short and swollen appearance of the cone OS (**Fig. 3a,** red and white arrows, respectively). Although not apparent by immunohistochemistry in mouse RPE, human RPE cells express functional MYO1C [29], and low levels of *Myo1C* mRNA appear present in mouse RPE [30]. Since elimination of the motor protein *Myo7a* in mouse leads to alterations in protein localization in the RPE (RPE65) [31], we stained retinas of young and adult WT and *Myo1c*-KO mice with anti-STRA6 antibody, another RPE-specific protein. This analysis suggests that STRA6 expression and localization in the RPE was not affected in the absence of MYO1C (**Fig. 4b**). Thus, since MYO1C is known primarily as a motor with protein trafficking function [14, 18], its absence in photoreceptors of *Myo1c*-KO animals may contribute specifically to the loss of opsin trafficking to the OS.

***Myo1c*-KO Mice demonstrate Photoreceptor Outer Segment Loss**: To further evaluate if opsin mistrafficking is also associated with structural changes to the retina, the histological and TEM analysis of retinal sections of young and adult WT and *Myo1c*-KO mice was performed. In histological sections of H&E stained tissues, progressive shortening of rod photoreceptor OS was observed, where the OS of adult *Myo1c*-KO (6 months of age) mice appeared shorter than the younger *Myo1c*-KO mice (2 months of age), which in turn were shorter than those in WT mice (**Fig. 4a**). Also, in comparison to the WT mice, the photoreceptors in *Myo1c*-KO mice appeared to be less organized, especially in the older mice (**Fig. 4a**), suggesting that loss of MYO1C may affect progressively affect photoreceptor homeostasis. To further evaluate the structure of rod photoreceptors, ultrastructural analysis using TEM was performed. While the rod photoreceptor OS in the WT mice showed normal elongated morphology, they appeared shorter and wider in *Myo1c*-KO mice at two months of age (**Fig. 4b**). Specifically, comparing *Myo1c*-KO with WT mouse rod outer segment lengths at six months of age demonstrated that OS segment lengths in *Myo1c* retinas were 35-48% shorter than those of WT mice ($P<0.005$; **Fig. 4c**). TEM analysis of *Myo1c*-KO mice retinas at six months of age for rod structure showed that they were significantly shorter in lengths ($P<0.05$; **Fig. 4d *vs* 4e;** rod lengths quantified in **Fig. 4f**, at two months and **Fig. 4g**, at 6 months). Ultra-structurally, the cone outer segments in the *Myo1c*-KO mouse retina appeared shorter and had lost their typical cone shape, confirming the swollen shape identified by immunohistochemistry. Retinal lamination and nuclear cell layers in *Myo1c*-KO mice however, appeared normal (**Fig. 4a**). These results suggest

that the lack of MYO1C resulted in progressively severe opsin mislocalization (**Figs. 2** and **3**), shorter photoreceptor OS (**Fig. 4**), supporting the observed decrease in visual function by ERG (**Figs. 1b-e**).

MYO1C Cargo Domain directly Interacts with Rhodopsin: Since the loss of MYO1C resulted in retinal function defects with significant alterations in the localization of opsins, we evaluated whether MYO1C exerts this effect through a physical interaction with rhodopsin. Immunoprecipitation analysis using WT and *Myo1c*-KO (*n* = 6 retinas pooled per genotype) mice demonstrated that rhodopsin was pulled down using MYO1C antibody and in a reciprocal fashion (**Figs. 5a** and **5b**). Using a baculovirus produced purified recombinant mouse MYO1C protein, we further demonstrate that MYO1C directly interacted with rhodopsin in an overlay assay, where opsin immunoprecipitated either from mouse retinal lysate or HEK293 cells overexpressing Myo1c, and separated on an SDS-PAGE gel and then probed with purified recombinant full-length MYO1C (MYO1C FL) or GFP-MYO1C-790-1028 (tail domain, also known as the cargo domain) [13]. The immunoblot analysis of the over-layered MYO1C showed significant binding of both MYO1C proteins, full-length and tail, at the rhodopsin band indicating a direct interaction between the two proteins (**Fig. 5**). Interestingly, the interaction of MYO1C was noted with various multimers of rhodopsin, which further indicates that opsin is a cargo for MYO1C (**Fig. 5**).

Genetic Deletion of *Myo1c* does not affect Systemic Organs in Mice: Finally, to determine if the systemic deletion of *Myo1c* affects other organs, we harvested major

systemic organs, including liver, heart, and kidney of 6 months old *Myo1c*-KO and WT mice (*n*=5 per genotype), and performed histology and H&E staining. Notably, both young and adult *Myo1c*-KO mice developed and reproduced normally with no observable differences between the control and *Myo1c*-KO genotypes (**Figs. S5a-c**). Thus, except for the retinal phenotype, *Myo1c*-KO animals showed unremarkable pathology of systemic organs.

Discussion:

Our work identifies for the first time an unconventional motor protein, MYO1C, as a novel trafficking regulator of both rod and cone opsins to the photoreceptor OS in mice. In this study, based on MYO1C localization within the IS and OS of photoreceptors, and using a whole-body *Myo1c*-KO mouse model, we have functionally identified MYO1C as a novel component of retinal physiology, where it was specifically found to be involved in photoreceptor cell function. Retinal analysis of *Myo1c*-KO mice identified opsins as novel cargo for MYO1C. In the absence of MYO1C, both young and adult *Myo1c*-KO mice showed impaired opsin trafficking, where rhodopsin was retained in the photoreceptor IS and the cell bodies. In contrast, cone opsins showed no retention in the cell body or mistrafficking of other membranes, but staining pattern revealed misformed cone OS. These two phenotypes manifested in a progressive decline of visual responses in both the rod and cone ERGs and shorter photoreceptor OS as *Myo1c*-KO animals aged, indicating a progressive phenotype. Significantly, only a retinal phenotype was observed, as systemic organs of *Myo1c*-KO mice, including heart, liver, and kidney, appeared unaffected. Our data thus points to a novel

mechanism by which MYO1C regulates opsins trafficking from the photoreceptor IS to OS, which is a critical event for photoreceptors' function and long-term photoreceptor cell survival. Our study identifies an unconventional motor protein MYO1C, as an essential component of the mammalian photoreceptors, which plays a critical role in promoting phototransduction and long-term photoreceptor cell survival.

MYO1C is Involved in Photoreceptors function via the Transport of opsins from Inner segments to Outer Segments: Photoreceptor degeneration has devastating consequences on visual function. Therefore, protein trafficking, in particular appropriate trafficking of both rod and cone opsins within the photoreceptors must occur efficiently and at high fidelity for normal photoreception, proper structural maintenance, and for overall retinal cellular homeostasis. However, some of the molecular players remain unknown, and therefore is an area of intense research. Herein, the identification of mechanisms that contribute to opsin trafficking, and consequently to the integrity of photoreceptors may help design protective/therapeutic strategies to restore photoreceptor function in humans with inherited retinal degenerative diseases. The observation that MYO1C is involved in opsin trafficking suggest that this protein could be explored/targeted as a therapeutic modality to mitigate retinal degenerative diseases, especially in patients with defective opsin trafficking.

MYO1C and other Opsin Trafficking Proteins*: Myo1c*-KO mice exhibited rhodopsin mislocalization similar to *Rpgr*$^{-/-}$, *Myo7a*^{Sh1}, *Rp1*$^{-/-}$, *Kinesin II*$^{-/-}$, and *Tulp1*$^{-/-}$ mutant mice [1-9]. And just like in these mutant mice, the *Myo1c*-KO mice showed opsin

mislocalization and shorter OS with little or no photoreceptor cell death up to the 6-month time point of analysis. Since MYO1C primarily localized to photoreceptor IS and OS, is known to be involved in protein trafficking and uses actin as a track [14, 18], we hypothesized that MYO1C participates in the movement of opsins from IS to the OS of photoreceptors. This hypothesis was supported by the observation that the rod opsins were mislocalized to IS and cell bodies and defective assembly of cone OS in *Myo1c*-KO mice suggests that this phenotype is caused by an aberrant protein transport and that OS degeneration was likely a secondary event. Apparently, the normal ultrastructure of photoreceptors in our *Myo1c*-KO mice suggests that the retinal abnormalities in these animals are not due to structural defects in photoreceptors per se, but instead are induced by an aberrant motor function leading to opsin mislocalization.

MYO1C contributes to Phototransduction and Retinal Homeostasis: The opsin molecules and other phototransduction proteins are synthesized in the cell body of the photoreceptor [32, 33]. They are then transported to the distal IS [34], and subsequently to the OS. Little is known about these transport processes and the molecular components involved in this process [1-9]. The localization of MYO1C in the photoreceptors' IS and OS, suggests that opsins may utilize this molecular motor for transport to the OS. The immunohistochemical analysis of *Myo1c*-KO animals indicated that while rod and cone opsins trafficked to the OS, significant mislocalization was noted for rhodopsin in the IS and cell bodies in the ONL (**Fig. 2**). Since they represent plasma membrane structural proteins, cone opsins presumably contribute to the cone OS

stability and rhodopsin to the rod OS formation and stability [7], and hence photoreceptor OS degeneration in *Myo1c*-KO mice may be attributed, in large part, to the mistrafficking of opsins to the IS or to a progressive reduction of opsins in the OS membrane. Notably, the pattern of opsin mislocalization observed in *Myo1c*-KO mice resembled closely with the retinal phenotype observed in our previously reported *Tulp1*-KO, [4, 35], *Cnga3*$^{-/-}$ mice [5], *Lrat*$^{-/-}$ and *Rpe65*$^{-/-}$ [3, 8, 9], GC1-KO mice [1, 6], and, to some extent in CFH (complement factor H) KO animals [2]. Importantly, in all these studies, photoreceptor OS was unstable, and significant degeneration was noted. However, because 85-90% of OS protein is rhodopsin, the mislocalization of other less abundant proteins cannot be ruled out in the photoreceptors of *Myo1c*-KO mice.

Contributions from other Motor proteins in Opsin trafficking: Though the study demonstrates mistrafficking of opsins due to a loss of MYO1C, the majority of opsin was still correctly localized, suggesting that contribution or compensation from other myosins cannot be ruled out. Nevertheless, the contributions from MYO1C are highly significant, as its genetic deletion showed specific physiological defects in mouse retinas. It is likely that some redundancy exists among molecular motors and several known candidates might compensate for the lack of MYO1C in photoreceptor function. However, the qPCR analysis of the retinas from WT and *Myo1c-KO* mice did not suggest compensation from other family myosin 1 members (**Fig. S6**). However, compensation by other motor proteins, including the members of kinesin superfamily [36, 37], myosin VIIa, and conventional myosin (myosin II) [38, 39], which have also been detected in the RPE and retina, cannot be ruled out and may need further investigation. Overall, results

presented herein support a role for MYO1C in opsin trafficking in the photoreceptor cells of the retina and provide evidence that defective protein transport pathways may be a pathologic mechanism responsible for OS degeneration and loss of vision, in these mice.

Methods:

Materials: All chemicals, unless stated otherwise, were purchased from Sigma-Aldrich (St. Louis, MO, USA) and were of molecular or cell culture grade quality.

***Myo1c*-Knockout (*Myo1c*-KO) Mouse Model**: We have previously generated *Myo1c* transgenic mice (*Myo1cfl/fl*) in C57BL/6N-derived embryonic stem cells, flanking exons 5 to 13 of the mouse *Myo1c* gene, which has allowed us to specifically delete all *Myo1c* isoforms in a cell-specific manner [24]. Here, a complete *Myo1c*-knockout was generated by crossing *Myo1cfl/fl* mice with an F-actin Cre mouse strain (B6N.FVB-Tmem163Tg(ACTB-cre)2Mrt/CjDswJ) obtained from Jackson labs. We will refer to the *Myo1cfl/fl* x f-actin Cre cross as *Myo1c* knockout (*Myo1c*-KO) mice. For this study, the *Myo1c*-KO mice were crossed onto a C57BL/6J background to avoid potential problems with the *Rd8* mutation (found in C57BL/6N lines) [40].

Immunohistochemistry and Fluorescence Imaging: Eyes were fixed in 4% paraformaldehyde buffered with 1X PBS for 2 hours at 4^0C using established protocols [58]. After fixation, samples were washed in PBS and embedded in paraffin and processed (MUSC histology core facility). Sections (10 µm) were cut and transferred onto frost-free slides. Slide edges were lined with a hydrophobic marker (PAP pen) and

washed with PBS before blocking for 1-2 hr at RT. Blocking solution (1% BSA, 5% normal goat serum, 0.2% Triton-X-100, 0.1% Tween-20 in 1X PBS) was applied for 2 hours in a humidified chamber. Primary antibodies were diluted in blocking solution as follows: anti-rhodopsin (1:500, Millipore/Sigma, St. Louis, MO), anti-Myo1c (1:100), cone-arrestin (1:250, Millipore/Sigma, St. Louis, MO), conjugated PNA-488 and PNA-594 (1:2000, Molecular Probes, Eugene, OR), anti-red/green cone opsin (1:500; Millipore, St. Louis, MO), anti-S-opsin (1:500, Millipore/Sigma, St. Louis, MO), and 4′,6-diamidino-2-phenylendole (DAPI; 1:5000) was used to label nuclei. All secondary antibodies (Alexa 488 or Alexa 594) were used at 1:5000 concentrations (Molecular Probes, Eugene, OR). Optical sections were obtained with a Leica SP8 confocal microscope (Leica, Germany) and processed with the Leica Viewer software.

Measurement of Photoreceptor Outer Nuclear Layer (ONL) Thickness and Outer Segment (OS) Lengths: All fluorescently labeled retinal sections on slides were analyzed by the program BIOQUANTNOVA (R & M Biometrics, Nashville). The length of the photoreceptor OS and thickness of the ONL were measured at five consecutive points in a 100 μm segment located 300-400 μm from the optic nerve. The ONL thickness was measured from the base of the nuclei to the outer limiting membrane at a 90° angle. The OS length was measured from the base of the OS to the inner side of the retinal pigment epithelium. Only sections in which columns of rod nuclei were apparent were counted to ensure that sections were not oblique. Measurements from the four quadrants (see above) were averaged; the SD was less than 10% of the average value for each mouse.

Electroretinography (ERG) Analysis: Dark-adapted WT and *Myo1c*-KO mice (50:50 ratio of male and female*; n*=8 each genotype) at two months of age (young mice; early time-point), and between 6-7 months of age (end time-point) were anesthetized by intraperitoneal injection of a ketamine/xylene anesthetic cocktail (100 mg/kg and 20 mg/kg, respectively) and their pupils were dilated with 1% tropicamide and 2.5% phenylephrine HCl. Both scotopic and photopic ERGs were recorded with a computerized system (UTASE-3000; LKC Technologies, Inc., Gaithersburg, MD, USA), as previously described [41-43].

Transmission Electron Microscopy (TEM): Eyecups at the indicated time-points were harvested and fixed overnight at 4^0C in a solution containing 2% paraformaldehyde/2.5% glutaraldehyde (buffered in 0.1M cacodylate buffer). Samples were then rinsed in the buffer (0.1 M cacodylate buffer). Post-fixative 2% OsO_4/0.2 M cacodylate buffer 1 hour at 4^0C, followed by 0.1 M cacodylate buffer wash. The samples were dehydrated through a graded ethanol series and then embedded in epon (EMbed 812; EM Sciences). The cured blocks were cut at 0.5 microns and stained with 1% toluidine blue to orient the blocks to the required specific cell types. The blocks were then trimmed to the precise size needed for ultrathin sectioning. The blocks were cut at 70 nm and gathered on 1-micron grids. The grids were air-dried and then stained with uranyl acetate (15 minutes) and lead citrate (5 minutes) and rinsed in-between each stain. They were then allowed to dry and imaged with a JEOL 1010. Images were acquired with a Hamamatsu camera and software. All samples were processed by the

Electron Microscopy Resource Laboratory at the Medical University of South Carolina, as previously described [53,70].

Western Blot Analysis and Densitometry: Total protein from cells or mouse tissues (*n*=3 per genotype) were extracted using the M-PER protein lysis buffer (ThermoScientific, Beverly, MA) containing protease inhibitors (Roche, Indianapolis, IN). Approximately 25 μg of total protein was then electrophoresed on 4-12% SDS-PAGE gels and transferred to PVDF membranes. Membranes were probed with primary antibodies against anti-Myo1c (1:250), β-Actin or Gapdh (1:10,000, Sigma), in antibody buffer (0.2% Triton X-100, 2% BSA, 1X PBS) [54,55,70]. HRP conjugated secondary antibodies (BioRad, Hercules, CA) were used at 1:10,000 dilution. Protein expression was detected using a LI-COR Odyessy system, and relative intensities of each band were quantified (densitometry) using Image J software version 1.49 and normalized to their respective loading controls.

Co-immunoprecipitation Assays: Co-immunoprecipitation of endogenously expressed proteins (MYO1C and rhodopsin) was performed using mouse retinal extracts. Six retinas of each genotype (WT and *Myo1c*-KO) were used for extraction of retinal proteins in 250 μL of RIPA buffer (phosphate-buffered saline [PBS] containing 0.1% sodium dodecyl sulfate [SDS], 1% Nonidet P-40, 0.5% sodium deoxycholate, and 100 mM potassium iodide) with EDTA-free proteinase inhibitor mixture (Roche Molecular Biochemicals). Lysates were cleared by centrifugation at 10000 rpm for 10 min at 4°C. The prepared lysates were incubated with anti-Myo1c, anti-rhodopsin, and

mouse/rabbit IgG overnight at 4°C and further with protein G-coupled agarose beads (ROCHE) for 1-2 h. Beads were then collected by centrifugation at 3000 rpm for 5 min at 4°C, extensively washed in 1X PBS, and resuspended in SDS gel loading buffer. The proteins were separated on a 10% SDS-PAGE, transferred to a PVDF membrane, and analyzed by immunoblotting with the corresponding antibodies.

Overlay direct binding assay: Rhodopsin protein was expressed in HEK293 cells using transient transfection (pcDNA3 rod opsin construct, a gift from Robert Lucas (Addgene plasmid # 109361, http://n2t.net/addgene:109361; RRID:Addgene_109361) [44] and immunoprecipitated from the cell lysates using an anti-rhodopsin antibody (Abcam). In parallel, rhodopsin was similarly immunoprecipitated from the mouse retinal lysate. The immunoprecipitated complexes were separated on SDS-PAGE gel and transferred to PVDF membrane. The membrane was then probed by overlaying it with 5 µg of baculovirus-produced and purified recombinant full-length MYO1C FL or GFP-MYO1C-790-1028 (tail domain, also known as the cargo domain [13]) protein and incubating at 4^0C for 4 h. Following incubation, the membranes were western blotted with MYO1C antibody to detect the direct binding of MYO1C to the rhodopsin bands. The location of rhodopsin on the membranes was marked by separately probing these membranes with an anti-rhodopsin (1:500, Millipore Sigma) antibody.

Quantitative Real Time-PCR: RNA was isolated from retinas of WT and *Myo1c*-KO animals using Trizol reagent, and processed as described previously [55,70]. One microgram of total RNA was reverse transcribed using the SuperScript II cDNA

Synthesis Kit (Invitrogen, Eugene, OR). Quantitative Real-Time PCR (qRT-PCR) was carried out using SYBR green 1 chemistry (BioRad, Hercules, CA). Samples for qRT-PCR experiments were assayed in triplicate using the BioRad CFX96 Q-PCR machine. Each experiment was repeated twice (n=6 reactions for each gene), using newly synthesized cDNA.

Statistical Analysis: Data are expressed as means ± standard deviation by ANOVA in the Statistica 12 software (StatSoft Inc., Tulsa, Oklahoma, USA). Differences between means were assessed by Tukey's honestly significant difference (HSD) test. P-values below 0.05 ($P<0.05$) were considered statistically significant. For western blot analysis, relative intensities of each band were quantified (densitometry) using the Image J software version 1.49 and normalized to the loading control β-Actin. QRT-PCR analysis was normalized to 18S RNA, and the ΔΔCt method was employed to calculate fold changes. Q-RTPCR data are expressed as mean ± standard error of mean (SEM). Statistical analysis was carried out using PRISM 8 software-GraphPad.

DATA AVAILABILITY

The authors declare that all data supporting the finding of this study are available within this article and its supplementary information files or from the corresponding author upon request. The plasmids will be available from the corresponding author upon reasonable request.

Disclosure

All the authors declared no competing interests.

Acknowledgements

This work was supported by grants from the NIH/NEI R21EY025034, R01EY030889, Medical University of South Carolina (MUSC) start-up funds, and a Dialysis Clinic, Inc. (award DCI-019898-001) research grant to G.P.L. 2R01DK087956-06A1, R56-DK116887-01A1 and 1R03TR003038-01 to D.N. VA (Merit Award I01 BX000820), NIH (P30DK074038), Dialysis Clinic, Inc. (research grant), and the American Heart Association (AWRP Winter 2017 Collaborative Sciences Award) to J.H.L. This project was also supported in part by the South Carolina Clinical and Translational Research (SCTR) Institute at the Medical University of South Carolina, NIH/NCATS grant number 5UL1TR001450 to G.P.L.

Author Contributions

G.P.L., and D.N., designed the research studies. G.P.L., A.K.S., B. Rohrer., S.H., J.S., J.H.L., and D.N. wrote and edited the manuscript. G.P.L., A.K.S., E.O., D.N., E.A., S.W., S.H., and B.R. conducted experiments and acquired data. A.K.S., E.O., G.P.L., E.A., B. Rohrer., S.H., J.S., and D.N., analyzed and interpreted the data. B. Rohrer., J.S., S.H., and J.H.L., supplied reagents and provided equipment for data analysis. All authors have read and agreed to the published version of the manuscript.

Figure Legends

Fig. 1: MYO1C localizes to photoreceptors in mouse retina and its genetic deletion induces vision defects: (**a**) Retina from adult wild-type (WT) and *Myo1c*-KO mice were harvested and immunostained with an anti-MYO1C antibody followed by secondary (Alexa 488) antibody staining. Dark-adapted scotopic ERGs were recorded in response to increasing light intensities in cohorts of two-month-old control (Wild-type/WT (white box)) and *Myo1c*-KO (black box) mice (**b, c**) and six months old (**d, e**) mice. Two-month-old *Myo1c* knock-out mice had lower dark-adapted *a*- and *b*-wave amplitudes compared with controls (post-hoc ANOVA: *a*-waves, $p < 0.0068$; *b*-waves, $p < 0.0098$), in particular at higher light intensities (20, 10, 6, 0 db). Six-month-old *Myo1c* knock-out mice had lower dark-adapted *a*- and *b*-wave amplitudes compared with controls (post-hoc ANOVA: *a*-waves, $p < 0.005$; *b*-waves, $p < 0.005$), in particular at higher light intensities (20, 10, 6, 0 db). Photoreceptor cell responses (*a*-waves), which drive the *b*-waves, were equally affected in *Myo1c*-KO animals (both reduced on average between 38-45% to WT animals). Data are expressed as mean ± S.E. (*Myo1c*-KO mice, $n = 8$; WT mice, $n = 8$). RPE, retinal pigmented epithelium; OS, outer segments; IS, inner segments; ONL, outer nuclear layer.

Fig. 2: Immunohistochemical analysis of wild-type/WT and *Myo1c* knock-out mice retina shows opsin trafficking defects: (**a**) Levels and localization of rhodopsin (Rho); **b***,* red/green (M-opsin); cone opsins (*green,* cone opsin); **c,** short wavelength (S-opsin); **d,** Pde6b; and **e,** PNA-488 in were analyzed from two and six months old WT and *Myo1c-KO* mice retinas. *Arrows* in ***a*** highlight rhodopsin mislocalization in *Myo1c* knock-out mouse retinas.

Fig. 3: Immunohistochemical analysis of protein trafficking in RPE and photoreceptors of wild-type/WT and *Myo1c* knock-out mice retinas: (**a**) Levels and localization of cone arresting (ARR); **b***,* STRA6, were analyzed from two- and six-months old WT and *Myo1c-KO* mice retinas to evaluate protein trafficking to photoreceptor outer segments or within the RPE. *Red Arrows* in ***a*** highlight cone photoreceptor nuclei, while *White Arrows* in ***a*** highlight cone photoreceptor OS in WT mouse retinas that were significantly reduced or shorter respectively in *Myo1c-KO* animals.

Fig. 4: Histological, H&E staining, and ultrastructural analysis shows reduced OS length of *Myo1c*-KO mice retinas: Retinas from two and six months old *Myo1c-KO* and WT mice (**a**) were sectioned and stained with H&E to evaluate pathological consequences of MYO1C loss. Ultrastructural analysis using transmission electron microscopy (TEM) of rod photoreceptors from two months old WT and *Myo1c-KO* mice (**b**), from six months old WT and *Myo1c-KO* mice (**c**) and cones from six months old mice for (**d, e**) are presented. Quantification of rod OS lengths (**f,** two months old mice; **g,** six months old). Rod (**b, c**) and cone (**d, e**) outer segment lengths were quantified based on the thickness of the respective outer segment areas. Scale bar=2um (**b, c**). Scale bar=800 nm (**d, e**).

RPE, retinal pigmented epithelium OS, outer segments; IS, inner segments; ONL, outer nuclear layer; INL, inner nuclear layer; OPL, outer plexiform layer; IPL, inner plexiform layer; GCL, ganglion cell layer.

Fig. 5: Rhodopsin is a direct cargo for MYO1C: (**a**) Using Rhodopsin antibody, Rhodopsin (RHO) was immunoprecipitated either from mice retinal lysates or from HEK293 cells where it was overexpressed, (**b**) and separated on SDS-PAGE and transferred to PVDF membrane. The membrane was then incubated with 5ug of purified recombinant active MYO1C-full length (**a**) or MYO1C C-terminal cargo domain protein (**b**) generated from baculovirus expression system. The blots were then western blotted with MYO1C antibody, which showed direct binding of MYO1C to various Rhodopsin multimers present in the retinal lysate and overexpressed HEK293 cells.

Supplementary Figures

Fig. S1: Western blot analysis of MYO1C in systemic tissues: Western blot analysis confirmed MYO1C absence in various systemic tissues of *Myo1c*-KO mice. Absence of MYO1C did not affect MYO1B or MYO1E expression. Actin was used as the protein loading control.

Fig. S2: MYO1C expression in mouse tissue by immunofluorescence: Expression of MYO1C in systemic tissues, kidney (**a**), liver (**b**), and heart (**c**) of WT and *Myo1c*-KO animals by immunofluorescence. WT, wild type; KO, knockout.

Fig. S3: Quantification of OS lengths and distribution of Opsins in *Myo1c* knock-out photoreceptors at two months of age: Cone lengths **(a)** and rhodopsin distribution within rod IS **(b)** and IS **(c)** were quantified based on the thickness of the respective outer segment areas. Approximately 500 cones in 5-6 retinal sections from each animal (n=8 animals; both genotypes) were sized. For quantification of rhodopsin distribution, 3-5 retinal sections from each animal (n=8 animals; both genotypes) were assayed. Mann-Whitney *U* test was used for statistical analysis and represented in Box-Whisker plots and considered significant $P<0.05$.

Fig. S4: Quantification and Distribution of Opsins in *Myo1c* knock-out photoreceptors at six months of age: Cone lengths **(a)** and rhodopsin distribution within rod IS **(b)** and IS **(c)** were quantified based on the thickness of the respective outer segment areas and fluorescence in different retinal layers. Approximately 500 cones in 5-6 retinal sections from each animal (n=8 animals; both genotypes) were sized. For quantification of rhodopsin distribution, 3-5 retinal sections from each animal (n=8 animals; both genotypes) were assayed. Mann-Whitney *U* test was used for statistical analysis and represented in Box-Whisker plots and considered significant $P<0.05$.

Fig. S5: Representative tissue histology and staining of systemic organs from WT and *Myo1c*-KO animals. Systemic organs, liver (**a**), kidney (**b**), and heart (**c**), of *Myo1c* and WT animals were sectioned and stained with H&E to evaluate any pathological consequences of systemic MYO1C loss.

Fig. S6: qPCR analysis of various MYO1C family members in mice retina: Retinas from WT and Myo1c-KO mice were isolated and processed for qPCR analysis using specific primers for various *Myo1c* family members including *Myo1b, d, e and f*.

References

1. Baehr, W., et al., *The function of guanylate cyclase 1 and guanylate cyclase 2 in rod and cone photoreceptors.* J Biol Chem, 2007. **282**(12): p. 8837-47.
2. Coffey, P.J., et al., *Complement factor H deficiency in aged mice causes retinal abnormalities and visual dysfunction.* Proc Natl Acad Sci U S A, 2007. **104**(42): p. 16651-6.
3. Fan, J., et al., *Rpe65-/- and Lrat-/- mice: comparable models of leber congenital amaurosis.* Invest Ophthalmol Vis Sci, 2008. **49**(6): p. 2384-9.
4. Grossman, G.H., et al., *Immunocytochemical evidence of Tulp1-dependent outer segment protein transport pathways in photoreceptor cells.* Exp Eye Res, 2011. **93**(5): p. 658-68.
5. Hüttl, S., et al., *Impaired channel targeting and retinal degeneration in mice lacking the cyclic nucleotide-gated channel subunit CNGB1.* J Neurosci, 2005. **25**(1): p. 130-8.
6. Karan, S., et al., *A model for transport of membrane-associated phototransduction polypeptides in rod and cone photoreceptor inner segments.* Vision Res, 2008. **48**(3): p. 442-52.
7. Pearring, J.N., et al., *Protein sorting, targeting and trafficking in photoreceptor cells.* Prog Retin Eye Res, 2013. **36**: p. 24-51.
8. Zhang, H., et al., *Trafficking of membrane-associated proteins to cone photoreceptor outer segments requires the chromophore 11-cis-retinal.* J Neurosci, 2008. **28**(15): p. 4008-14.
9. Zhang, T., et al., *Cone opsin determines the time course of cone photoreceptor degeneration in Leber congenital amaurosis.* Proc Natl Acad Sci U S A, 2011. **108**(21): p. 8879-84.
10. Abdelkader, E., et al., *Severe retinal degeneration at an early age in Usher syndrome type 1B associated with homozygous splice site mutations in MYO7A gene.* Saudi J Ophthalmol, 2018. **32**(2): p. 119-125.
11. Cheng, L., et al., *Identification of a novel MYO7A mutation in Usher syndrome type 1.* Oncotarget, 2018. **9**(2): p. 2295-2303.
12. Arif, E., et al., *Motor protein Myo1c is a podocyte protein that facilitates the transport of slit diaphragm protein Neph1 to the podocyte membrane.* Mol Cell Biol, 2011. **31**(10): p. 2134-50.
13. Nakamori, Y., et al., *Myosin motor Myo1c and its receptor NEMO/IKK-gamma promote TNF-alpha-induced serine307 phosphorylation of IRS-1.* J Cell Biol, 2006. **173**(5): p. 665-71.
14. Woolner, S. and W.M. Bement, *Unconventional myosins acting unconventionally.* Trends Cell Biol, 2009. **19**(6): p. 245-52.
15. Walsh, T., et al., *From flies' eyes to our ears: mutations in a human class III myosin cause progressive nonsyndromic hearing loss DFNB30.* Proc Natl Acad Sci U S A, 2002. **99**(11): p. 7518-23.
16. Rehman, A.U., et al., *Mutational Spectrum of MYO15A and the Molecular Mechanisms of DFNB3 Human Deafness.* Human mutation, 2016. **37**(10): p. 991-1003.
17. Adamek, N., M.A. Geeves, and L.M. Coluccio, *Myo1c mutations associated with hearing loss cause defects in the interaction with nucleotide and actin.* Cellular and molecular life sciences : CMLS, 2011. **68**(1): p. 139-150.
18. Adamek, N., M.A. Geeves, and L.M. Coluccio, *Myo1c mutations associated with hearing loss cause defects in the interaction with nucleotide and actin.* Cell Mol Life Sci, 2011. **68**(1): p. 139-50.
19. Lin, T., et al., *A hearing loss-associated myo1c mutation (R156W) decreases the myosin duty ratio and force sensitivity.* Biochemistry, 2011. **50**(11): p. 1831-8.
20. Skeie, J.M. and V.B. Mahajan, *Proteomic interactions in the mouse vitreous-retina complex.* PLoS One, 2013. **8**(11): p. e82140.

641 21. Boguslavsky, S., et al., *Myo1c binding to submembrane actin mediates insulin-induced tethering*
642 *of GLUT4 vesicles.* Mol Biol Cell, 2012. **23**(20): p. 4065-78.
643 22. Bose, A., et al., *Unconventional myosin Myo1c promotes membrane fusion in a regulated*
644 *exocytic pathway.* Mol Cell Biol, 2004. **24**(12): p. 5447-58.
645 23. Fan, Y., et al., *Myo1c facilitates G-actin transport to the leading edge of migrating endothelial*
646 *cells.* J Cell Biol, 2012. **198**(1): p. 47-55.
647 24. Arif, E., et al., *The motor protein Myo1c regulates transforming growth factor-beta-signaling and*
648 *fibrosis in podocytes.* Kidney Int, 2019.
649 25. Crosson, C.E., et al., *Inhibition of histone deacetylase protects the retina from ischemic injury.*
650 Invest Ophthalmol Vis Sci, 2010. **51**(7): p. 3639-45.
651 26. Husain, S., D.E. Potter, and C.E. Crosson, *Opioid receptor-activation: retina protected from*
652 *ischemic injury.* Invest Ophthalmol Vis Sci, 2009. **50**(8): p. 3853-9.
653 27. Krebs, W. and H. Kühn, *Structure of isolated bovine rod outer segment membranes.* Exp Eye Res,
654 1977. **25**(5): p. 511-26.
655 28. Pearring, J.N., et al., *Protein sorting, targeting and trafficking in photoreceptor cells.* Progress in
656 retinal and eye research, 2013. **36**: p. 24-51.
657 29. Brandstaetter, H., et al., *Loss of functional MYO1C/myosin 1c, a motor protein involved in lipid*
658 *raft trafficking, disrupts autophagosome-lysosome fusion.* Autophagy, 2014. **10**(12): p. 2310-23.
659 30. Mustafi, D., et al., *Photoreceptor phagocytosis is mediated by phosphoinositide signaling.* FASEB
660 journal : official publication of the Federation of American Societies for Experimental Biology,
661 2013. **27**(11): p. 4585-4595.
662 31. Lopes, V.S., et al., *The Usher 1B protein, MYO7A, is required for normal localization and function*
663 *of the visual retinoid cycle enzyme, RPE65.* Human molecular genetics, 2011. **20**(13): p. 2560-
664 2570.
665 32. Young, R.W., *The renewal of photoreceptor cell outer segments.* J Cell Biol, 1967. **33**(1): p. 61-72.
666 33. Young, R.W. and B. Droz, *The renewal of protein in retinal rods and cones.* J Cell Biol, 1968. **39**(1):
667 p. 169-84.
668 34. Findlay, J.B. and D.J. Pappin, *The opsin family of proteins.* Biochem J, 1986. **238**(3): p. 625-42.
669 35. Lobo, G.P., et al., *Involvement of Endoplasmic Reticulum Stress in TULP1 Induced Retinal*
670 *Degeneration.* PLoS One, 2016. **11**(3): p. e0151806.
671 36. Beech, P.L., et al., *Localization of kinesin superfamily proteins to the connecting cilium of fish*
672 *photoreceptors.* J Cell Sci, 1996. **109 (Pt 4)**: p. 889-97.
673 37. Muresan, V., et al., *Evidence for kinesin-related proteins associated with the axoneme of retinal*
674 *photoreceptors.* Exp Eye Res, 1997. **64**(6): p. 895-903.
675 38. Chaitin, M.H. and N. Coelho, *Immunogold localization of myosin in the photoreceptor cilium.*
676 Invest Ophthalmol Vis Sci, 1992. **33**(11): p. 3103-8.
677 39. Williams, D.S., M.A. Hallett, and K. Arikawa, *Association of myosin with the connecting cilium of*
678 *rod photoreceptors.* J Cell Sci, 1992. **103 (Pt 1)**: p. 183-90.
679 40. Mattapallil, M.J., et al., *The Rd8 mutation of the Crb1 gene is present in vendor lines of C57BL/6N*
680 *mice and embryonic stem cells, and confounds ocular induced mutant phenotypes.* Invest
681 Ophthalmol Vis Sci, 2012. **53**(6): p. 2921-7.
682 41. Lobo, G.P., et al., *The exocyst is required for photoreceptor ciliogenesis and retinal development.*
683 J Biol Chem, 2017. **292**(36): p. 14814-14826.
684 42. Husain, S., *Delta Opioids: Neuroprotective Roles in Preclinical Studies.* J Ocul Pharmacol Ther,
685 2018. **34**(1-2): p. 119-128.
686 43. Husain, S., et al., *PI3K/Akt Pathway: A Role in delta-Opioid Receptor-Mediated RGC*
687 *Neuroprotection.* Invest Ophthalmol Vis Sci, 2017. **58**(14): p. 6489-6499.

44. Bailes, H.J. and R.J. Lucas, *Human melanopsin forms a pigment maximally sensitive to blue light (λmax ≈ 479 nm) supporting activation of G(q/11) and G(i/o) signalling cascades.* Proc Biol Sci, 2013. **280**(1759): p. 20122987.

Figure 1

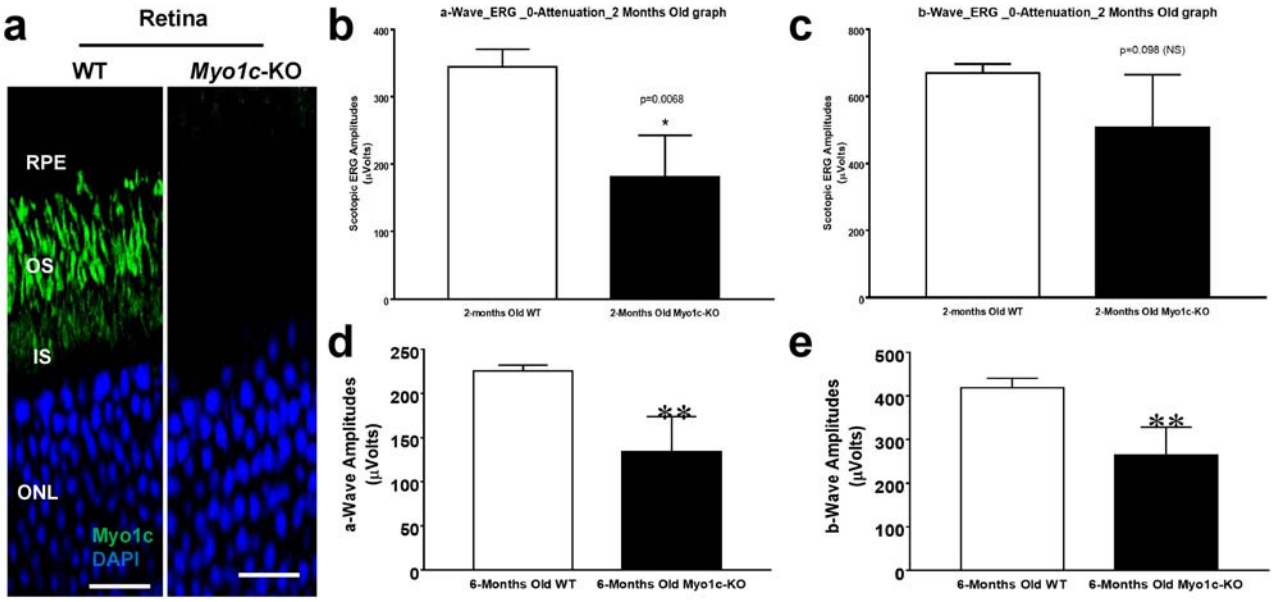

Figure 2

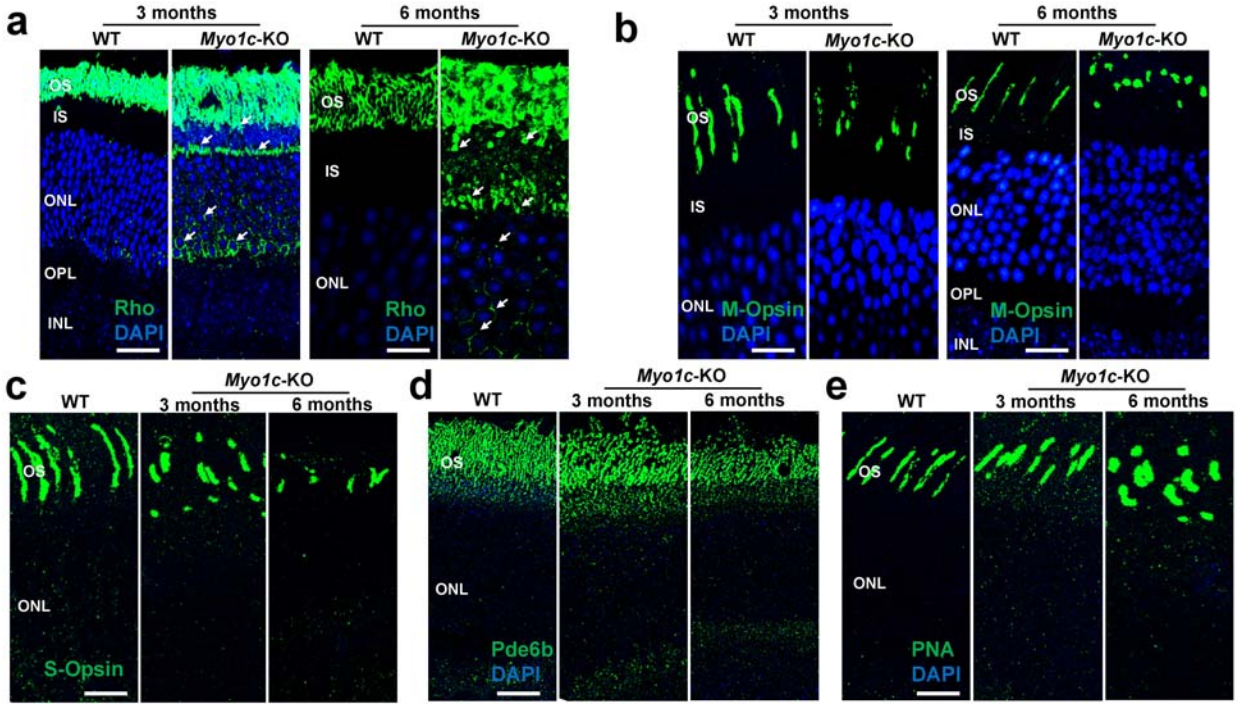
a
3 months
6 months
WT
Myo1c-KO
OS
IS
ONL
OPL
INL
Rho
DAPI
b
M-Opsin
c
S-Opsin
d
Pde6b
e
PNA

Figure 3

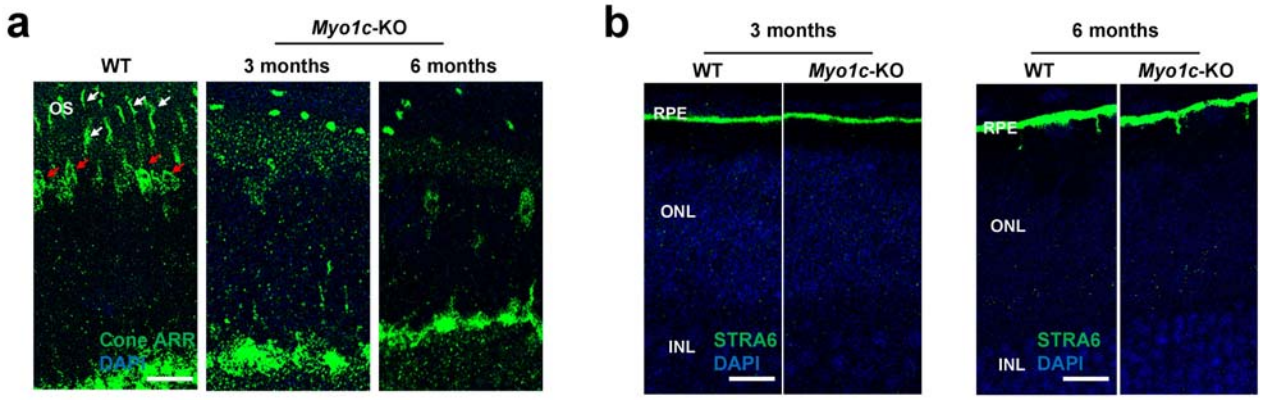
a
Myo1c-KO
WT
3 months
6 months
OS
Cone ARR
DAPI
b
3 months
6 months
WT
Myo1c-KO
RPE
ONL
INL
STRA6
DAPI

Figure 4

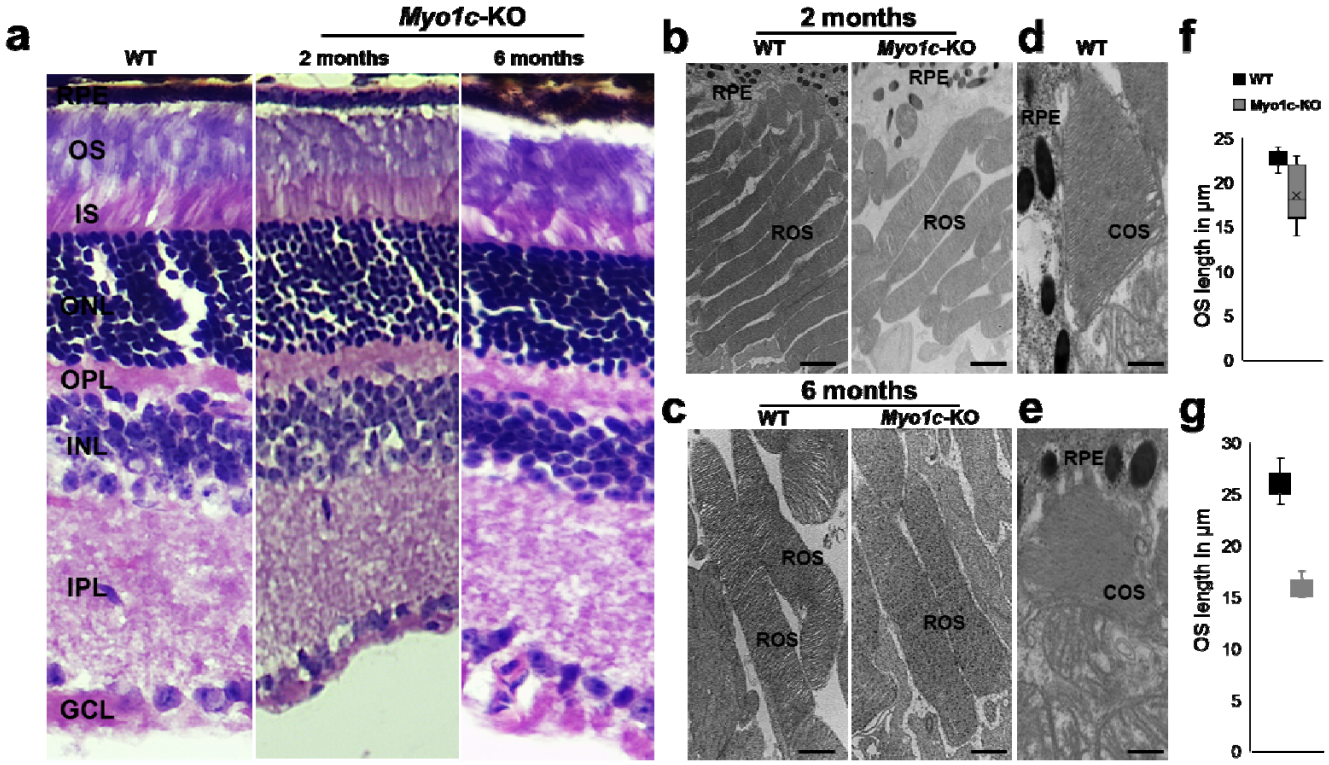
a
Myo1c-KO
WT
2 months
6 months
RPE
OS
IS
ONL
OPL
INL
IPL
GCL
b
2 months
WT
Myo1c-KO
RPE
ROS
c
6 months
WT
Myo1c-KO
ROS
d
WT
RPE
COS
e
RPE
COS
f
WT
Myo1c-KO
OS length in µm
25
20
15
10
5
0
g
OS length in µm
30
25
20
15
10
5
0

Figure 5

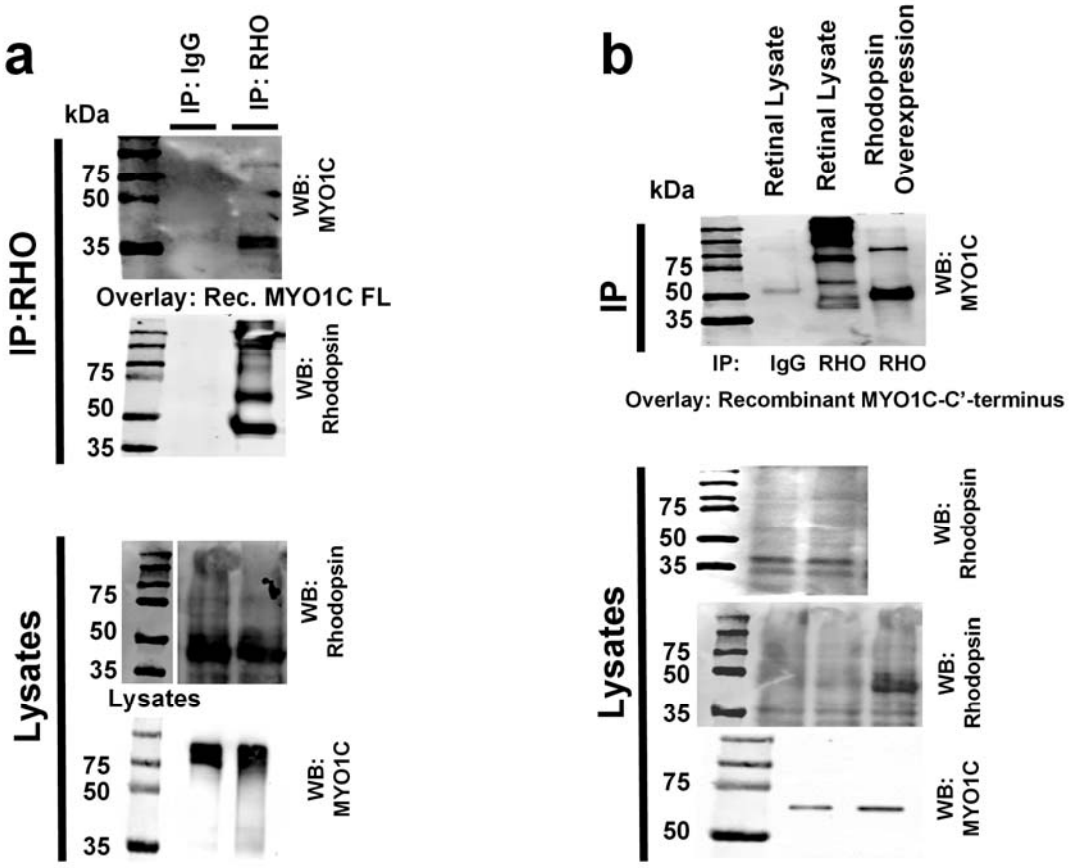
a
IP: IgG
IP: RHO
kDa
IP:RHO
75
50
35
WB: MYO1C
Overlay: Rec. MYO1C FL
WB: Rhodopsin
Lysates
Lysates
WB: MYO1C
b
Retinal Lysate
Retinal Lysate
Rhodopsin Overexpression
IP
IP: IgG RHO RHO
Overlay: Recombinant MYO1C-C'-terminus

Supplementary Figures:

Figure S1

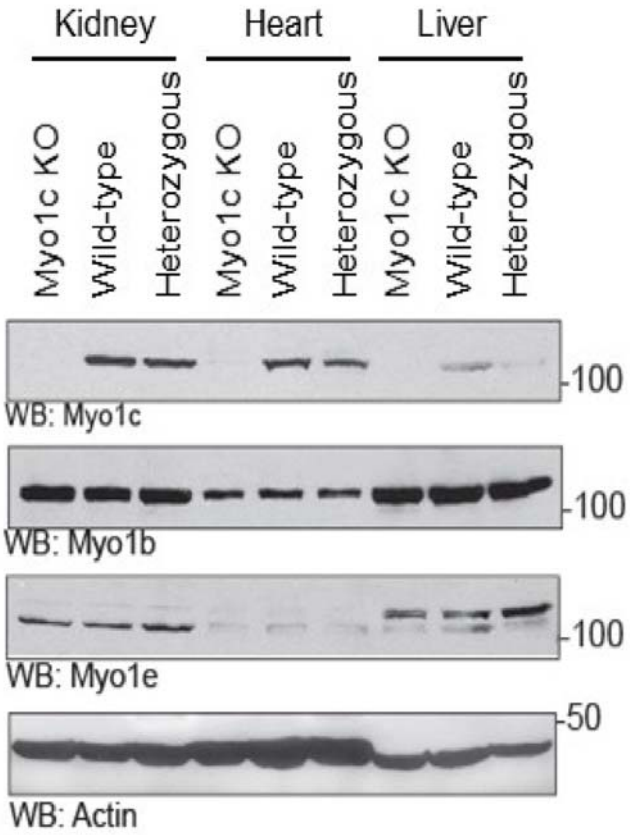

Figure S2

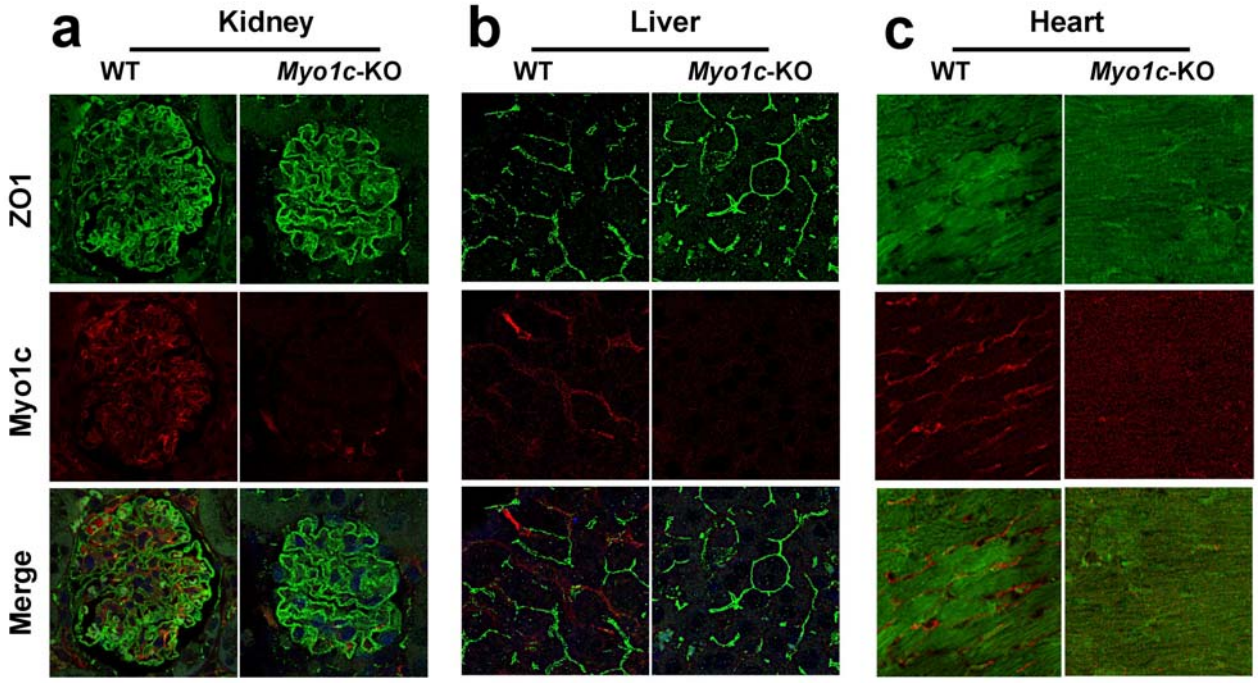
a
Kidney
WT
Myo1c-KO
b
Liver
WT
Myo1c-KO
c
Heart
WT
Myo1c-KO
ZO1
Myo1c
Merge

Figure S3

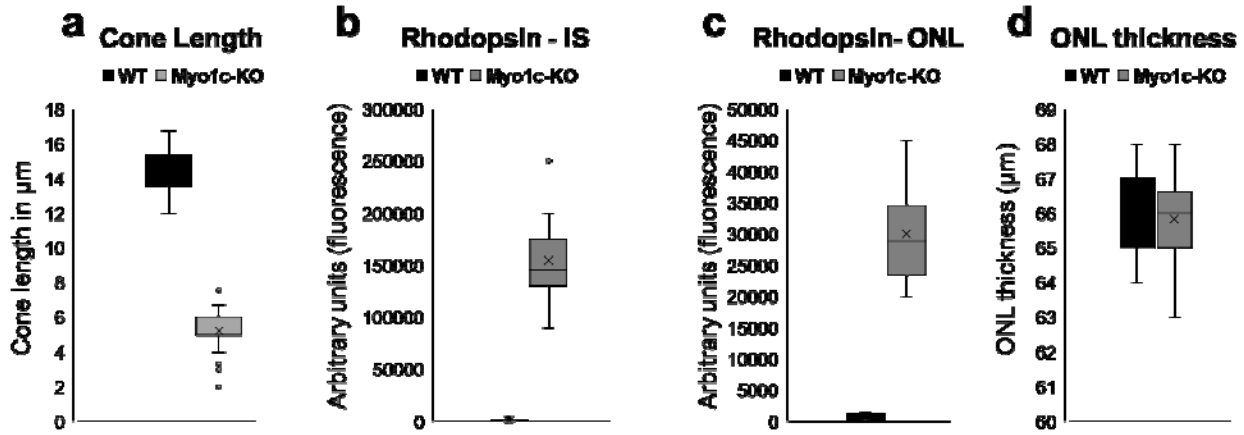
a
Cone Length
WT
Myo1c-KO
Cone length in µm
18
16
14
12
10
8
6
4
2
0
b
Rhodopsin - IS
WT
Myo1c-KO
Arbitrary units (fluorescence)
300000
250000
200000
150000
100000
50000
0
c
Rhodopsin- ONL
WT
Myo1c-KO
Arbitrary units (fluorescence)
50000
45000
40000
35000
30000
25000
20000
15000
10000
5000
0
d
ONL thickness
WT
Myo1c-KO
ONL thickness (µm)
69
68
67
66
65
64
63
62
61
60

Figure S4

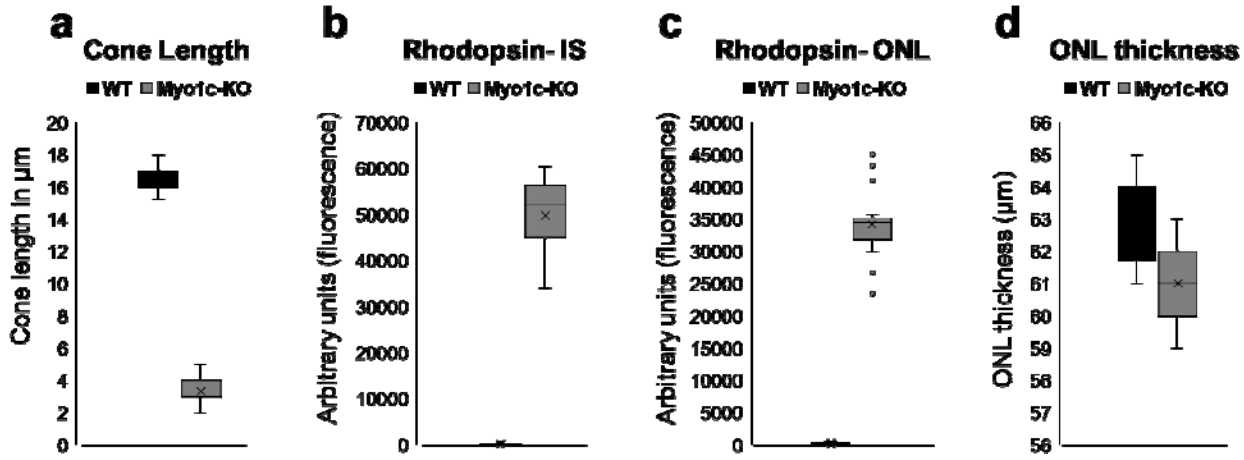
a
Cone Length
WT Myo1c-KO
Cone length in µm
20
18
16
14
12
10
8
6
4
2
0
b
Rhodopsin- IS
WT Myo1c-KO
Arbitrary units (fluorescence)
70000
60000
50000
40000
30000
20000
10000
0
c
Rhodopsin- ONL
WT Myo1c-KO
Arbitrary units (fluorescence)
50000
45000
40000
35000
30000
25000
20000
15000
10000
5000
0
d
ONL thickness
WT Myo1c-KO
ONL thickness (µm)
66
65
64
63
62
61
60
59
58
57
56

Figure S5

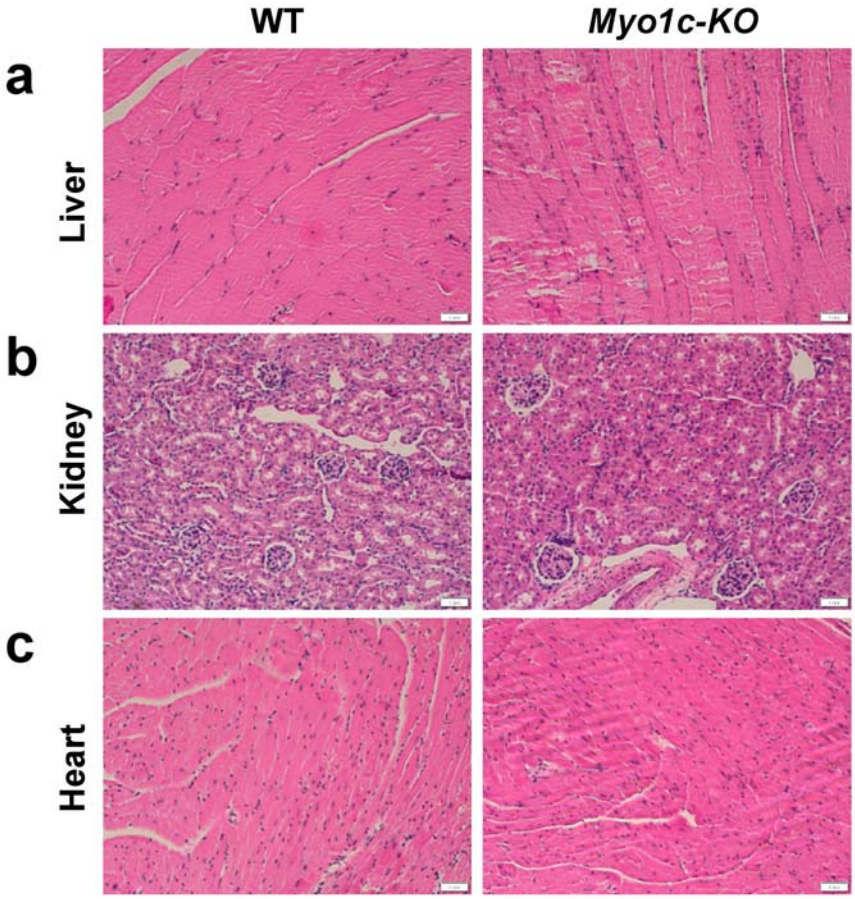

Figure S6

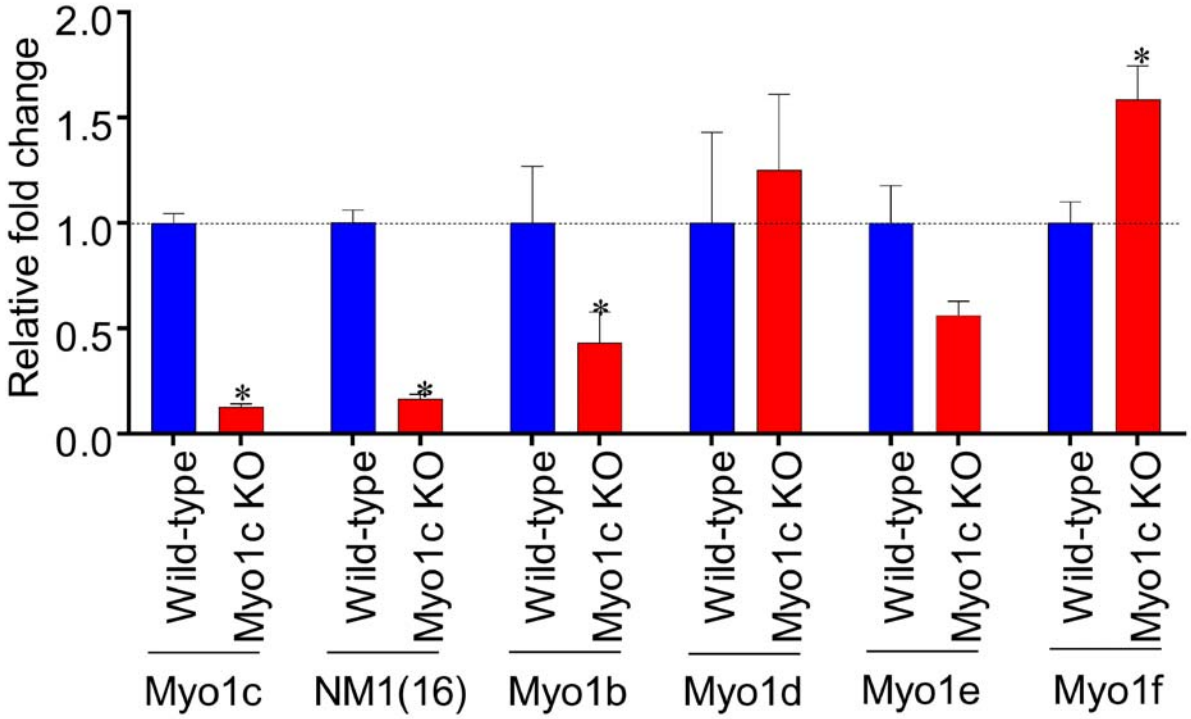

qPCR analysis from the eye sample isolated from wild-type and Myo1c knockout mice